Novel Annular Flow Electromagnetic Measurement System for Drilling Engineering

Liang GE, Guohui WEI, Qing WANG, Senior Member, IEEE，Ze HU, Junlan LI

***Abstract*—Downhole Micro-flux Control Drilling Technology can effectively solve drilling accidents such as kick and loss in narrow density window drilling scenarios. Using a downhole annular flow measurement system to obtain real time information of downhole annular flow is the core and foundation of Downhole Micro-flux Control Drilling Technology. The research work of electromagnetic flowmeters in recent years creates a challenge for downhole annular flow measurement. This paper proposes a new method for an annular flow measurement system based on the electromagnetic induction principle. First, the annular flow measuring principle, the weight function, the density of virtual current and the magnetic field of the annular flow electromagnetic measurement system are described. Second, the basic design of the annular flow electromagnetic measurement system is described. Third, model simulation and dynamic experiments on an annular flow electromagnetic measurement system are carried out. The simulation and experimental results show a linear relationship between the system output and the annular flow rate, and also verify the correctness of annular flow electromagnetic measurement theory.**

***Index Terms*—Annular flow measurement; Electromagnetic induction; Vector weight function; Density of virtual current; Electromagnetic flowmeter**

I. INTRODUCTION

With the continuous tension between oil and gas supply and demand, petroleum and gas exploration is developing very fast[1]. Drilling safety issues become increasingly prominent when exploring the complex and deep formation of wells. A blowout is the uncontrolled release of crude oil or natural gas from an oil well or gas well when formation pressure exceeds the pressure applied to it by the column of drilling or other fluids in the wellbore. The blowout will do great harm, not only causing serious pollution to the environment but also causing human casualties and economic loss.

Kick is the precursor of blowout. A sudden kick from the formation into the annular poses a serious risk to the safety of drilling. If not controlled, it may lead to a blowout. Therefore, detection of the early kick is crucial to control the formation pressure and minimize the possibility of a blowout occurring[2]. The conventional method of identifying the kick is based on the surface observation of the mud tank level, and this method has two main weak points. The first weak point is that there is a high probability of delay in kick detection, and the second point is that it cannot judge the type of kick. Although a lot of effort is being spent on improving these weaknesses, an efficient and effective method has yet to be developed[3].Downhole micro-flux control drilling technology can effectively solve drilling accidents such as kick and loss in narrow density window drilling scenarios. Down-hole monitoring techniques have a potential to detect a kick at its early stage, so it is important to study downhole annular flow measurement technology.

During the past decade, theories and methods of flow measurement have been developed in the aim of measuring downhole annular flow. In order to meet the special environment of downhole drilling, downhole space, pressure, temperature and fluid properties should be considered. Much work has been reported in downhole annular flow measurement since 2004, but no relevant mature instrument product has been produced. W. Han et al investigated downhole annular flow measurement technology based on Acoustic Doppler, and applied for a USA invention patent in 2005[4]. W.A. Mark developed a new downhole annular flow measurement technology based on Acoustic principles in 2011 and also applied for a USA invention patent[5]. J. Wei et al investigated the subsea ultrasonic annular flow measuring system using the principal of time difference and Doppler, and completed some relevant experiments in 2011[6].However, this kind of annular flow measuring system cannot measure non-Newtonian fluids with large numbers of solid particles. P. Chen developed a downhole annular flow measuring system based on a differential pressure type flow measurement in 2012, and completed a downhole site test[7-8].A downhole differential pressure annular flow measuring system can be widely applied, and as it is almost completely insensitive to fluid properties it can be used in two-phase or multiphase flow. However, due to the chock part in measuring system, it will cause pressure loss and blocking problems in the chock part. This can be a major drawback, particularly in the safety of the drilling and precision of the measurement. Over recent years, there have been great environmental concerns about the electromagnetic flowmeter[9-10], and many researchers have carried out studies on the theories and simulation of annular flow electromagnetic measurement[11-13]. W.H. Cui et al. [11] developed a new method for multi-information acquisition from the electromagnetic flowmeter by using magnetic excitation to measure the fluid velocity and electrochemistry impedance spectroscopy. However, these studies have mainly focused on the situation of flowpath existing in the internal electrode and excitation system, without considering the particular situation

of flowpath existing outside of the electrode and excitation system. It is worth emphasizing that there is no literature reporting the use or research of the downhole annular flow electromagnetic measurement system for drilling engineering.

Electromagnetic measurement is ideally suited for measuring solid-liquid two-phase flow and other extremely difficult to measure fluids, and it does not have a chock part. Its operating principles provide flow measurement with a signal that is linear to the average volumetric flow rate, regardless of fluid temperature, pressure, density, viscosity or direction. The only limitation is that the fluid must have some electrical conductivity. Therefore, in this work, a downhole annular flow electromagnetic measurement system for drilling engineering was proposed, the sufficient and necessary conditions for the weight function, the density of the virtual current and the magnetic field were derived and calculated. Dynamic experiments on the annular flow electromagnetic measurement system were carried out, and the data were analyzed.

II. THEORY MODEL OF THE ANNULAR TWO-ELECTRODE FLOW ELECTROMAGNETIC MEASUREMENT SYSTEM

A. Response model of the annular flow electromagnetic measurement system

The measurement principle of the electromagnetic flowmeter is based on Faraday's Law, and the potential between two signal electrodes fulfills the integral equation, which can be expressed as follows[14]:

$$U = \int_{\tau} W \cdot \vec{v} d\tau \quad (1)$$

where W is given by: $W = \vec{B} \times \vec{j}$

Here, U is the potential between two electrodes, W is the weight function vector, $\vec{v}$ is velocity of the annular flow, $\vec{B}$ is the magnetic flux vector, $\vec{j}$ is the virtual current vector, and τ is the integration of annular volume. We may note from equation (1) that the response of the annular flow electromagnetic measurement system is fundamentally related to the weight function vector W and the annular flow velocity $\vec{v}$.The velocity of the annular flow weight function vector W is dependent on the magnetic flux density $\vec{B}$ and virtual current vector $\vec{j}$.

Generally, there is no electric power and magnetic source inside the annular flow electromagnetic measurement system, so the electrical potential G and magnetic potential F within the flow area satisfy the Laplace' equations:

$$\nabla^2 G = 0 \qquad \nabla^2 F = 0 \quad (2)$$

And the virtual current density $\vec{j}$ and magnetic flux vector $\vec{B}$ can be further denoted by:

$$\vec{j} = -\nabla G \qquad \vec{B} = -\nabla F \quad (3)$$

In real applications, the annular flow velocity is measured. Therefore the main goal of downhole annular flow electromagnetic measurement system research is to obtain the virtual current density $\vec{j}$ and magnetic flux vector $\vec{B}$.

B. Virtual current density of the annular two-electrode flow electromagnetic measurement system

Virtual current density characterizes the current density on condition that the 1 A current passes from the positive electrode to the negative electrode. In fact, the current does not exist in the flowpath of the electromagnetic flowmeter, and thus this current is called "virtual current". The distribution of virtual current density is dependent on the flowpath's shape, flow conductivities and the size and position of measuring electrodes[17-22].

Fig.1 shows a schematic diagram of the downhole annular two-electrode flow electromagnetic measurement system and the flowpath. A and B represent two electrodes placed on the outside wall at intervals of 180° inside the annular flowpath, N and S represent two magnetic coils inlaid on the wall of the annular flowpath at intervals of 180°,a and b are the distances of the inner and outer surfaces to the center, and∑1 and∑2 represent the inner and outer surfaces of the annular flowpath.

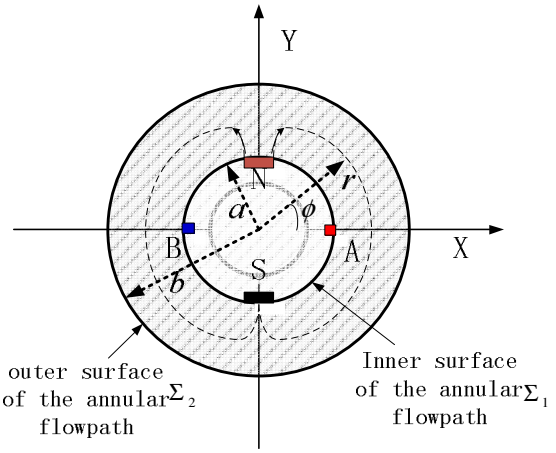

Fig.1 Schematic diagram of the annular two-electrode flow electromagnetic measurement system and the flowpath

To simplify the boundary conditions, we suppose that the electronic conductivity of the outer surface of the annular flowpath is much smaller than the flow. The partial differential equation and the boundary conditions of the outer surface of the annular flowpath and electrodes can be written as follows:

$$\begin{cases} \dfrac{\partial^2 G}{\partial r^2}+\dfrac{1}{r}\dfrac{\partial G}{\partial r}+\dfrac{1}{r^2}\dfrac{\partial^2 G}{\partial \phi^2}=0 \\ \left.\dfrac{\partial G}{\partial r}\right|_{r=b}=0 \\ \left.\dfrac{\partial G}{\partial r}\right|_{r=a}=\begin{cases}\delta(\phi-\phi_A)/a \\ -\delta(\phi-\phi_B)/a\end{cases} \end{cases} \quad (4)$$

Where $\phi_A=0$ and $\phi_B=\pi$ are the angular position of electrodes A and B. Using the segregation variable method, equation(4) can be expressed as:

$$\begin{cases} r^2\dfrac{d^2R}{dr^2}+r\dfrac{dR}{dr}-KR=0 \\ \dfrac{d^2\Phi}{d\phi^2}+K\phi=0 \end{cases} \quad (5)$$

When $K=n^2$, by solving differential equations, the results can be written as:

$$\begin{cases} R=C_0+D_0\ln r+\sum\limits_{n=1}^{\infty}\left(C_n r^n+D_n r^{-n}\right) \\ \Phi=\sum\limits_{n=1}^{\infty}\left(A_n\sin n\phi+B_n\cos n\phi\right) \end{cases} \quad (6)$$

Equation(6) can be transformed into the following equation:

$$G=C_0+D_0\ln r+\sum_{n=1}^{\infty}\left(C_n r^n+D_n r^{-n}\right)\left(A_n\sin n\phi+B_n\cos n\phi\right) \quad (7)$$

$$\frac{\partial G}{\partial r}=D_0\frac{1}{r}+\sum_{n=1}^{\infty}nr^{-n-1}\left(C_n r^{2n}-D_n\right)\left(A_n\sin n\phi+B_n\cos n\phi\right) \quad (8)$$

For the boundary condition $\left.\partial G/\partial r\right|_{r=b}=0$,so that:

$$D_0=0 \quad D_n=C_n b^{2n} \quad (9)$$

By substituting equation(9) into equation (7) and equation (8),we have:

$$G=C_0+\sum_{n=1}^{\infty}C_n\left(r^n+b^{2n}r^{-n}\right)\left(A_n\sin n\phi+B_n\cos n\phi\right) \quad (10)$$

$$\frac{\partial G}{\partial r}=\sum_{n=1}^{\infty}nr^{-n-1}C_n\left(r^{2n}-b^{2n}\right)\left(A_n\sin n\phi+B_n\cos n\phi\right) \quad (11)$$

When the angular positions $\phi_A=0$ and $\phi_B=\pi$,for the boundary condition $\left.\partial G/\partial r\right|_{r=a}=\delta(\phi)/a$,we have:

$$A_n=0\ B_n=\frac{a^n}{n\pi C_n\left(a^{2n}-b^{2n}\right)} \quad (12)$$

thus:

$$G_1(r,\phi)=C_0+\frac{1}{\pi}\sum_{n=1}^{\infty}\frac{(a/b)^n(r/b)^n+(a/r)^n}{n\left[(a/b)^{2n}-1\right]}\cos n\phi \quad (13)$$

Similarly, when the angular positions $\phi_A=0$ and $\phi_B=\pi$,for the boundary condition $\left.\partial G/\partial r\right|_{r=a}=-\delta(\phi-\pi)/a$,we have:

$$A_n=0\ B_n=\frac{-a^n\cos n\pi}{n\pi C_n\left(a^{2n}-b^{2n}\right)} \quad (14)$$

thus:

$$G_2(r,\phi)=C_0-\frac{1}{\pi}\sum_{n=1}^{\infty}\frac{(a/b)^n(r/b)^n+(a/r)^n}{n\left[(a/b)^{2n}-1\right]}\cos n\phi\cos n\pi \quad (15)$$

Here, we suppose that C0 is 0.Combination equation(13)and equation(15) together, G can be written as:

$$G=G_1+G_2=\frac{2}{\pi}\sum_{n=1,3,5}^{\infty}\frac{(a/b)^n(r/b)^n+(a/r)^n}{n\left[(a/b)^{2n}-1\right]}\cos n\phi \quad (16)$$

Where $\tau=a/b$ 、 $R=r/b$, the final electrical potential G of the downhole annular two-electrode electromagnetic flowmeter in the cylindrical coordinate system can be expressed as follows:

$$G=\frac{2}{\pi}\sum_{n=1,3,5}^{\infty}\frac{R^n+R^{-n}}{n\left[\tau^n-\tau^{-n}\right]}\cos n\phi \quad (17)$$

Then we can obtain the virtual current density through the gradient operation, and the virtual current density can be expressed as follows:

$$\boldsymbol{j}=-\nabla G=-\left(\boldsymbol{e}_r\frac{\partial G}{\partial r}+\boldsymbol{e}_\phi\frac{1}{r}\frac{\partial G}{\partial \phi}\right) \quad (18)$$

$$\text{Wher, } j_r=-\frac{\partial G}{\partial r}=-\frac{2}{\pi a}\sum_{n=1,3,5}^{\infty}\frac{(a/b)^{n+1}(r/b)^{n-1}-(a/r)^{n+1}}{\left[(a/b)^{2n}-1\right]}\cos n\phi \quad (19)$$

$$j_\phi=-\frac{1}{r}\frac{\partial G}{\partial \phi}=\frac{2}{\pi a}\sum_{n=1,3,5}^{\infty}\frac{(a/b)^{n+1}(r/b)^{n-1}+(a/r)^{n+1}}{\left[(a/b)^{2n}-1\right]}\sin n\phi \quad (20)$$

Here $\tau=a/b$ 、 $R=r/b$, thus:

$$j_r=-\frac{2}{\pi b}\sum_{n=1,3,5}^{\infty}\frac{R^{n-1}-R^{-(n+1)}}{\left[\tau^n-\tau^{-n}\right]}\cos n\phi \quad (21)$$

$$j_\phi=\frac{2}{\pi b}\sum_{n=1,3,5}^{\infty}\frac{R^{n-1}+R^{-(n+1)}}{\left[\tau^n-\tau^{-n}\right]}\sin n\phi \quad (22)$$

When $\tau=0.3$, we obtain the isograph of electrical potential G in graph Fig.2when using equation(17).It can be seen from the plot that the maximum value of electrical potential in the annular flow domain is near the electrodes.

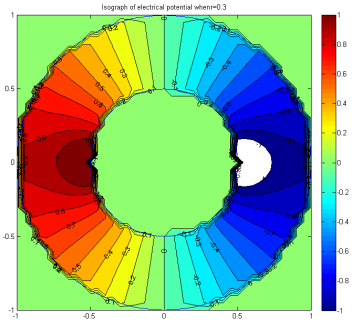

Fig.2 Isograph of electrical potential when τ =0.3

When $\tau=0.3$ and $b=1$, we obtain the isograph of virtual current density component j_r in Fig.3(a) when using

equation(21) and the isograph of virtual current density component j_ϕ in Fig.3 (b) when using Equation(22).

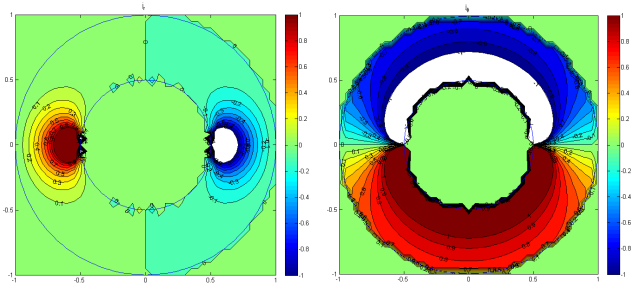

（a） j_r (b) j_ϕ

Fig.3 Isograph of virtual current density when $\tau = 0.3$ and $b = 1$

C. *Magnetic flux density of the annular two-coil flow electromagnetic measurement system*

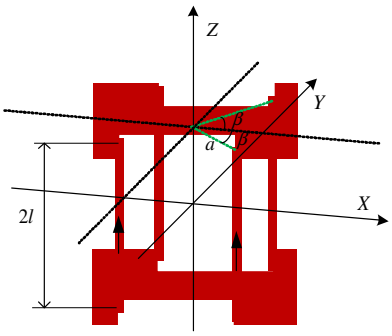

Fig.4 The structure a pair of Saddle coils

Fig.4 shows the structure of a pair of Saddle coils in a downhole annular two-electrode electromagnetic flowmeter. The direction of the coil current is shown in Fig.4, and the arc current angle is 2 β .

1)According to the superposition theorem of the field[15-16], the radical magnetic induction intensity of Saddle coils in annular space can be written as follows:

$$B_r = \sum_{i=1}^{4} B_{lir} + \sum_{i=1}^{4} B_{cir} \qquad (23)$$

Where:

$$B_{lir} = \frac{\mu I_i}{4\pi}\left[\frac{a\sin(\phi-\phi_i)}{(z+l)\sqrt{K_i^2+(z+l)^2}+K_i^2+(z+l)^2} - \frac{a\sin(\phi-\phi_i)}{(z-l)\sqrt{K_i^2+(z-l)^2}+K_i^2+(z-l)^2}\right] \qquad (24)$$

$$K_i = \sqrt{r^2+a^2-2ra\cos(\phi-\phi_i)} \qquad (25)$$

Here (ϕ_i, I_i) is $(\beta,-I)$、$(\pi-\beta,-I)$、$(\pi+\beta,I)$ and $(-\beta,I)$ respectively.

$$B_{cir} \approx \frac{\mu a I_i (z-z_i)}{4\pi}\sum_{\phi_k=\phi_{0i}}^{\phi_{0i}+2\beta}\frac{\cos(\phi-\phi_k)}{\left[r^2+a^2+(z-z_i)^2-2ar\cos(\phi-\phi_k)\right]^{3/2}} \qquad (26)$$

here (ϕ_{0i}, z_i, I_i) is $(-\beta,l,I)$、$(\pi-\beta,l,-I)$、$(\pi-\beta,-l,I)$ and $(-\beta,-l,-I)$ respectively.

2)Similarly, the circumferential Magnetic induction intensity of Saddle coils in annular space can be written as follows:

$$B_\phi = \sum_{i=1}^{4} B_{li\phi} + \sum_{i=1}^{4} B_{ci\phi} \qquad (27)$$

where：

$$B_{li\phi} = \frac{\mu I_i}{4\pi}\left[\frac{r-a\cos(\phi-\phi_i)}{(z-l)\sqrt{K_i^2+(z-l)^2}+K_i^2+(z-l)^2} - \frac{r-a\cos(\phi-\phi_i)}{(z+l)\sqrt{K_i^2+(z+l)^2}+K_i^2+(z+l)^2}\right] \qquad (28)$$

Here (ϕ_i, I_i) is $(\beta,-I)$、$(\pi-\beta,-I)$、$(\pi+\beta,I)$ and $(-\beta,I)$ respectively.

$$B_{ci\phi} = -\frac{\mu I(z-z_i)}{4\pi r}\left[\frac{1}{\sqrt{r^2+a^2+(z-z_i)^2-2ar\cos(\phi-\phi_{0i}-2\beta)}} - \frac{1}{\sqrt{r^2+a^2+(z-z_i)^2-2ar\cos(\phi-\phi_{0i})}}\right] \qquad (29)$$

Here (ϕ_{0i}, z_i, I_i) is $(-\beta,l,I)$、$(\pi-\beta,l,-I)$、$(\pi-\beta,-l,I)$ and $(-\beta,-l,-I)$ respectively.

3）The axial Magnetic induction intensity of Saddle coils in annular space can be written as follows:

$$B_z \approx \sum_{i=1}^{4}\frac{\mu I_i a}{4\pi}\sum_{\phi_k=\phi_{0i}}^{\phi_{0i}+2\beta}\frac{a-r\cos(\phi-\phi_k)}{\left(r^2+a^2+(z-z_i)^2-2ar\cos(\phi-\phi_k)\right)^{3/2}} \qquad (30)$$

Here (ϕ_{0i}, z_i, I_i) is $(-\beta,l,I)$、$(\pi-\beta,l,-I)$、$(\pi-\beta,-l,I)$ and $(-\beta,-l,-I)$ respectively.

III. FINITE ELEMENT MODEL

In order to verify feasibility of the theory model of annular flow electromagnetic measurement system, a finite element model was built based on the fundamental equations of electromagnetic flowmeters, as described in equation (2). These differential equation could be solved using a contemporary computational method with proper boundary conditions, which we discussed previously in the theory model. The simulation model of an annular flow electromagnetic measurement system is shown in Fig.5. This model was investigated using the 'Electric Currents' and 'magnetic fields' application modes of COMSOL Multi-physics with the 'time harmonic stationary linear solver' contained in the COMSOL'AC/DC' module. This solver calculates the distributions of the virtual current density and the local magnetic flux density in the computing annular domain.

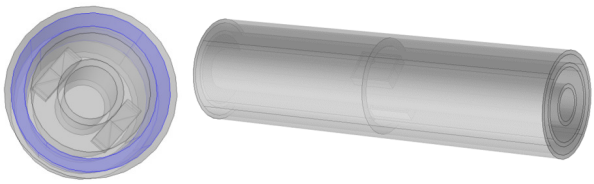

Fig. 5 The system simulation structure

Fig.6 shows the virtual current density distribution of the

annular flow electromagnetic measurement system. Through analysis, we can find that the virtual current density distribution is axis-symmetrical, and the virtual current density value of the point near the two electrodes is relatively large, while the other annular domain is small. This result is consistent with the previous theoretical study of virtual current density, as described in Fig.3.

Fig.7 shows a contour plot of the numerical calculation results of the magnetic flux density. The magnetic flux density value in annular area is not uniform, its value is depends on the coil sizes ,coil turns, coil current and coil position. It can be seen from the plot that the maximum value of the magnetic flux density in annular is around 1e-4 T from the coil positions, whereas the minimum value is near 2e-6 T from the electrode positions.

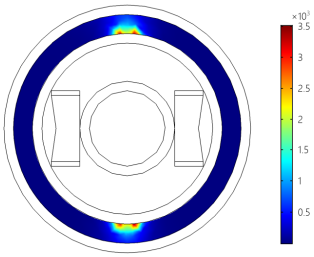

Fig. 6 The virtual current density（A/m^2）distribution

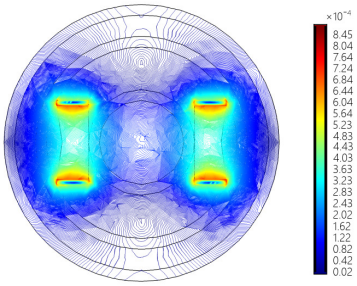

Fig.7 Contour plot of the numerical calculation results of the magnetic flux density(T)

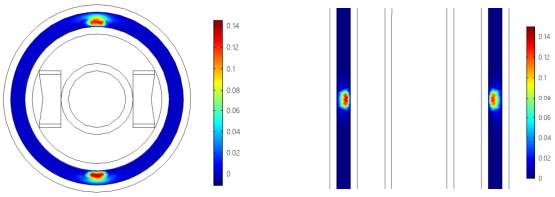

Fig.8 The induced electrical potential (V/m^3)distribution in XY plane(z=0) and YZ plane(x=0)

The induced electrical potential distribution within the annular channel can be calculated in different flow rates, and the induced electrical potential distribution is shown in Fig.8. The color distribution map changes from blue to red, representing the increase of induced electrical potential. In general, the values of induced electrical potential are relatively smaller in other positions of the annular area, especially for these positions far away from the coils and electrodes. The induced electrical potential distribution near the electrodes is relatively larger, and it indicates that this regions makes a larger contribution to the potential between two electrodes. It can be concluded that the induced electrical potential distribution is determined by the virtual current density and magnetic flux density together. The simulation result for flow rates varying from 13.0m^3/h to 101.6m^3/h is shown in Fig.16.

IV. System Design and Experimental Work

A. *The laboratory annular flow electromagnetic measurement system*

The Schematic diagram of the annular flow electromagnetic measurement system is shown in Fig.9.It is comprised of an annular electromagnetic flow detector module and an annular electromagnetic flow processor module. The annular electromagnetic flow detector module is the core of system. It is composed of a flow tube made of non-conducting PVC, a pair of electrodes and an electromagnet. The electrodes (0.7 mm in diameter and 18 mm in length) were made using molybdenum acid resistant steel, which has corrosion resistance and non-magnetic properties. The electromagnet is comprised of a pair if coils with 350 turns of enamel-coated copper wire of 1 mm diameter.

The annular electromagnetic flow processor is designed to accept analogue input from the annular electromagnetic flow detector. It mainly incorporates 5 parts[17-19]: a signal amplification and filtering part, a coil excitation part, a MCU part, a power supply part, and a data transmission interface part.

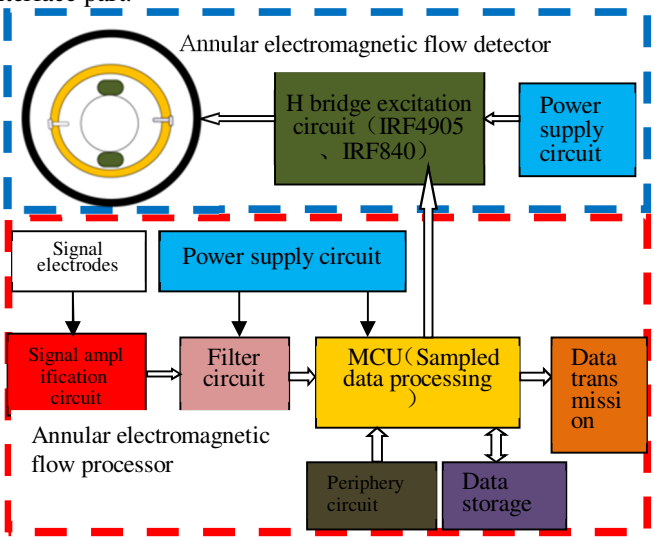

Fig.9 Schematic diagram of the annular flow electromagnetic measurement system

B. *Experimental work*

In order to evaluate the performance of the annular flow electromagnetic measurement system, an experimental flow loop system was conducted at State Key Laboratory of Oil & Gas Geology and Exploration at Southwest Petroleum University. The experimental flow loop system used for the experiments of the annular flow electromagnetic measurement system is shown schematically in Fig.10. The major components of the experimental flow loop system were a fluid reservoir, a valve, a bump, a surge tank, a frequency converter, an Electromagnetic Flowmeter, an annular device interface, a data acquisition system, some sensors and a transmitter.

The loop system working process was as follows[20-22]: firstly, the annular flow electromagnetic measurement system

was installed at the annular device interface of the loop system; then, the valve was opened and the flow was pumped ,the pressure of the flow was stabilized by passing through the surge tank; then, the flow was followed by flow rate measurement through a standard EMF, whose precision reached 0.5%; finally, the flow flowed through the laboratory annular flow electromagnetic measurement system and returned back to the fluid reservoir. During the experimental process, a personal computer with a data acquisition board named PCIE-8735 was used to measure the signals from the laboratory annular flow electromagnetic measurement system, sensors and transmitters.

A flow experiment is a complex operation that can easily introduce errors, which has a negative impact on the experimental data. Therefore, in order to make sure that a good quality experimental data were obtained, a careful and effective experimental procedure had to be designed. The experimental indoor conditions comprised normal pressure and temperature, and the experimental medium was running water. When the flow stabilized, the response values of the standard EMF and the annular flow electromagnetic measurement system were recorded. The total flow rates of the drilling fluid ranged from 13.0m^3/h to 101.6m^3/h. Data at 12 different flow rates were taken by comparing the standard EMF reading to the annular flow electromagnetic measurement system.

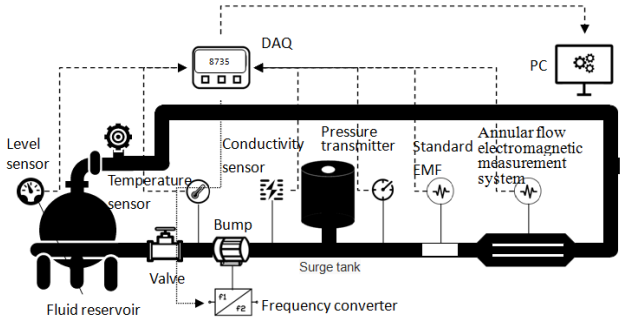

Fig.10 The diagram of the annular experimental facility

V. RESULTS

A. *Response characteristics of annular flow electromagnetic measurement system*

When the system excitation frequency is 1.84Hz, the output signal of annular flow electromagnetic measurement system after signal amplification and filtering can be obtained using the data acquisition board. Three typical wave curves of signal electrodes are shown from Fig.11 to Fig.13.

Fig.11 shows the output wave curve of the system when the annular flow path is no fluid or without fluid-filled. With close inspection of Fig.11,we can find that this signal wave is relatively independent of the flow rate. It is an interference signal due to the changes in electrode loop parameters and it originates from the excitation current switching and power frequency interference. This output wave curve can be used to estimate whether annular flow path is full of fluid or no fluid at all.

Fig.12 shows the output wave curve of the system when annular flow path is fluid-filled and there is zero flow rate. Through Fig.12, the zero reference voltage can be obtained by sampling the stable signal positions.

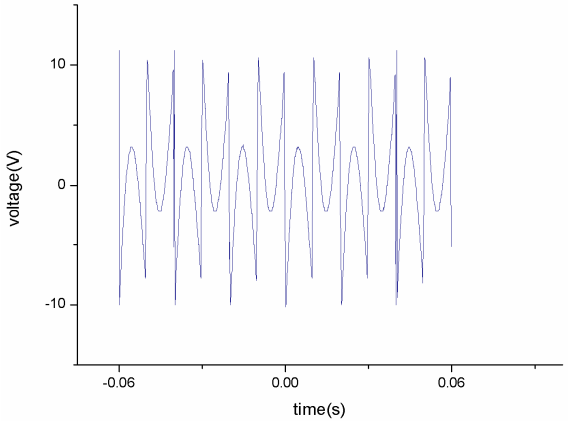

Fig.11 The output wave curve of the system when annular flow path is no fluid or without fluid-filled

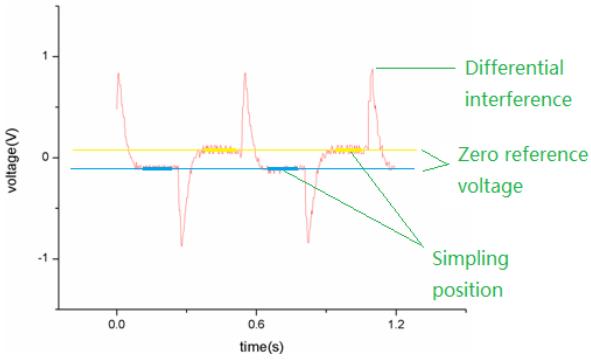

Fig.12 The output wave curve of system when the annular flow path is fluid-filled and there is zero flow rate

As shown in Fig.13,the effective amplitude of the waveform signal will change with the flow rate of the loop system changes. Through analysis, we can find that the output of the signal is in accordance with the former theory research and all the circuits and system work well. Though the loop system is relatively stable, the output of the signal cannot change immediately from one steady state to another because of the coil inductance and the noise. Furthermore, there are some fluctuations in the actual signal curve, which indicates that the signal is disturbed in some degree during the test. So it is worth pointing out that we need to avoid these interferences when extracting the flow signal.

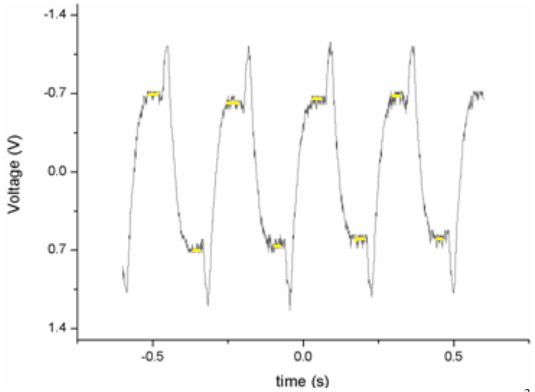

Fig.13 The wave curve of the system output (flow rate = 78.1 m^3/h)

B. Calibration and simulation result

A typical relation curve of the output voltage of annular electromagnetic flow measurement system and flow rate is shown in Fig.14. Figure 14 shows that the simulation result relation is a pure slope of a linear line, while the calibration result relation involves an intercept value which represents the reading of the annular flow electromagnetic measurement system despite a zero flow rate. These kind of zero reading refers to some fixed shift caused by noise or an electronic measuring circuit. The slopes of simulation result relation and calibration result relation are essentially the same, so the simulation model has the same system sensitivity as the annular flow electromagnetic measurement system.

The flow rate Q versus voltage U relationship obtained from the calibration data described above is found to be closely approximated by a linear equation(31) as follows:

$$Q = 58.8235 \times U - 7.2535 \quad (31)$$

Here, a=58.8235 and b=-7.2535 are the meter factors of the annular flow electromagnetic measurement system.

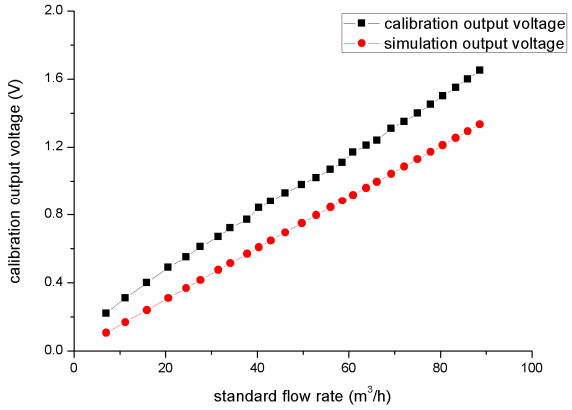

Fig.14 The calibration and simulation result of the annular flow electromagnetic measurement system

C. System test

After a calibration test, the meter factors were programmed into the measurement system, and an instantaneous flow value could be obtained directly. In this test, sex test points were chosen, and each test point was tested four times. The system-tested results are listed in Table 1. In order to evaluate the performances of the annular flow electromagnetic measurement system, tested results were analyzed and processed based on the verification regulation.

(1)Calculating the single time relative indication error of the measurement system for each test point by Equation (32):

$$E_{ij} = \frac{q_{ij} - (q_s)_{ij}}{(q_s)_{ij}} \times 100\% \quad (32)$$

Where, E_{ij} represents the jth relative indication error of measurement system belonging to the ith test point, %; q_{ij} represents the jth instantaneous flow of measurement system belonging to the ith test point, m^3/h; and $(q_s)_{ij}$ represents the jth instantaneous flow of Standard EMF belonging to the ith test point, m^3/h.

(2)Calculating the relative indication error of each test point of the measurement system using Equation (33):

$$E_i = \frac{1}{n}\sum_{j=1}^{n} E_{ij} \quad (33)$$

Where Ei represents the relative indication error of the ith test point of the measurement system, %; and n represents the verification times of the ith test point.

(3)Calculating the relative indication error of measurement system using Equation (34):

$$E = \pm |E_i|_{\max} \quad (34)$$

Here E will be the maximum relative indication error of the test points. All the single time relative indication error is listed in Table 1.

(4) Calculating the repeatability of each test point using Equation (35):

$$(E_r)_i = \sqrt{\frac{1}{n-1}\sum_{j=1}^{n}(E_{ij} - E_i)^2} \quad (35)$$

Where, Ei represents the relative repeatability of the ith test point of the measurement system, %; and Eij represents the jth relative indication error of the measurement system belonging to the ith test point, %.

(5)Calculating repeatability of the measurement system using Equation (36):

$$E_r = [(E_r)_i]_{\max} \quad (36)$$

Here Er will be the maximum repeatability of the test points.

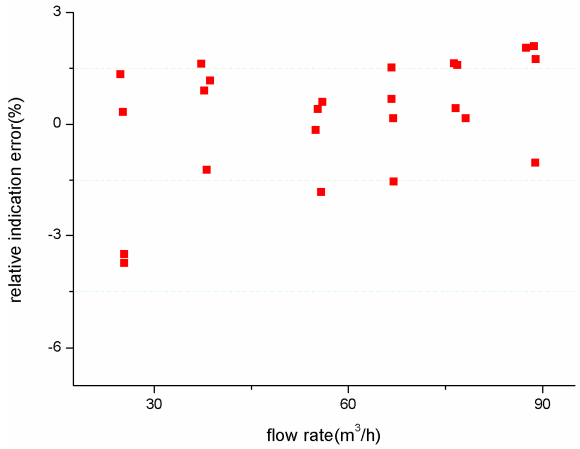

Fig.15 The single time relative indication error distribution

The single time relative indication error distribution of the test points is shown in Fig.15. Through Fig.15, we can find that the maximum single time relative indication error is -3.747%, and the minimum single time relative indication error is 0.149%. The single time relative indication error fluctuates around 0%. When the flow rate is less than about 25 m^3/h(the flow velocity in annular area is about 0.25m/s), system might easily lead to a bigger single time relative indication error. This problem is in accordance with the difficulty of low flow velocity measurement of EMF.

Based on the single time relative indication error, the mean relative indication error of each test point is calculated using

Equation（33）,and curve of the mean relative indication error of the test points is shown in Fig.16.According to Fig.16, we can find that the maximum mean relative indication error is -1.40%, and the minimum mean relative indication error is -0.25%. By comparison with single time relative indication error, the mean relative indication error of each test point is much smaller. Mean relative indication error of each test point could be decreased by taking mean value.

Table 1. Tested results of annular flow electromagnetic measurement system

Test points（converter frequency ,Hz）	Standard EMF（instantaneous flow,m^3/h）	System（instantaneous flow,m^3/h）	Flow difference（m^3/h）	Relative indication error（%）	Mean error（%）	Repeatability（%）
	24.84	24.51	0.33	1.329%		
14	25.18	25.1	0.08	0.318%	-1.40%	2.60%
	25.39	26.28	-0.89	-3.505%		
	25.39	26.86	-1.47	-3.747%		
	38.16	38.63	-0.47	-1.232%		
18	38.67	38.22	0.45	1.164%	0.61%	1.26%
	37.79	37.45	0.34	0.900%		
	37.29	36.69	0.6	1.609%		
	55.01	55.1	-0.09	-0.164%		
24	55.32	55.1	0.22	0.398%	-0.25%	1.09%
	56.02	55.69	0.33	0.589%		
	55.84	56.86	-1.02	-1.827%		
	66.96	66.86	0.1	0.149%		
28	66.7	65.69	1.01	1.514%	0.20%	1.29%
	67.01	68.04	-1.03	-1.537%		
	66.73	66.28	0.45	0.674%		
	78.16	78.04	0.12	0.154%		
32	76.91	75.69	1.22	1.586%	0.95%	0.77%
	76.6	76.28	0.32	0.418%		
	76.34	75.1	1.24	1.624%		
	88.89	89.81	-0.92	-1.035%		
36	87.48	85.69	1.79	2.046%	1.21%	1.50%
	89	87.45	1.55	1.742%		
	88.71	86.86	1.85	2.085%		

The repeatability of the test points is shown in Fig.17. Through Fig.17, we can find that the maximum repeatability is 2.60%, and the minimum repeatability is 0.77%.In general, a moderate flow rate leads to a better repeatability, and a bigger or a smaller flow rate leads to a worse repeatability.

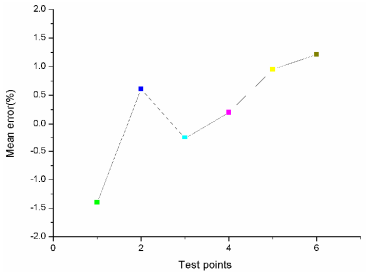

Fig.16 The mean relative indication error of the test points

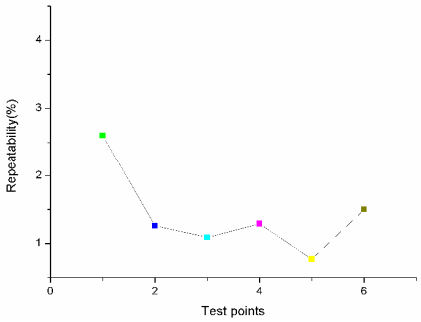

Fig.17 The repeatability of the test points

VI. CONCLUSION

This paper described a novel measuring technique for downhole annular flow. The following conclusions could be drawn according to the above-mentioned analysis and tests:

(1)The annular flow measuring principle, the weight function, the density of virtual current and the magnetic field of the annular flow electromagnetic measurement system for Drilling Engineering were described and analyzed.

(2)Finite element model was built based on the fundamental equations of electromagnetic flowmeter by COMSOL to verify the feasibility of the theory model of annular flow electromagnetic measurement system.

(3)The laboratory annular flow electromagnetic measurement system and experimental flow loop system were conducted, and experiments on it were carried out. The results of experiments showed that the annular flow electromagnetic measurement system researched in this study could be applied for flow rate measurement of downhole annular flow measurement while drilling.

ACKNOWLEDGMENT

This work is supported by the scientific research starting project of SWPU（No.2014QHZ029）, the National Natural Science Foundation(No.51504211) and the State Administration of National Security (No.sichuan-0011-2016AQ).

REFERENCES

[1]Anjum Aqeel and Mohammad Sabihuddin Butt, “The Relationship Between Energy Consumption And Economic Growth In Pakistan,” Asia-Pacific Development, vol. 8, no 8, pp.101-110,2001.

[2]John Kozicz. “Managed-Pressure Drilling-Recent Experience, Potential Efficiency Gains and Future Opportunities,” IADC/SPE Asia Pacific Drilling Technology Conference and Exhibition, Nov. 2006,SPE103753-MS, [Online].Available://www.onepetro.org/conference-paper/SPE-103753-MS.

[3]John W. Colbert and George Medley, “Light Annular MudCap Drilling - A Well Control Technique for Naturally Fractured Formations,” SPE Annual Technical Conference and Exhibition, Sep.2002,SPE-77352-MS,[Online].Available: //www.onepetro.org/conference-paper/SPE-77352-MS.

[4]W. Han and M.B. Jean, “Acoustic Doppler downhole fluid flow measurement,” U.S. Patent 6938458,Sep.6, 2005.

[5]W.A. Mark, “Annulus mud flow rate measurement while drilling and use thereof to detect well dysfunction,” U.S. Patent 7950451B2,May.31, 2011.

[6]J. Wei, et al, “Annular measurement device for subsea riser and drill string,” China Patent 102174887B,Jan.5,2011.

[7]L. Shi, P. Chen, Z. Hu and Y. J. Fu, “The Application of bottom-hole Flowmeter in the MPD system,” Journal of Southwest Petroleum University(Science &Technology Edition), vol. 32, no 6, pp 89-92, 2010.

[8]L. Ge et al, “Research on Overflow Monitoring Mechanism Based on Downhole Microflow Detection,”Mathematical Problems in Engineering, vol. 2014,pp 1-6, 2014.

[9]C.J. Bates, “Upstream installation and misalignment effects on the performance of a modified electromagnetic flowmeter,” Flow Measurement and Instrumentation, vol. 10, no 2, pp : 79-89,1999.

[10]Y.J Wang, et al, “Novel Downhole Electromagnetic Flowmeter for Oil-Water Two-Phase Flow in High-Water-Cut Oil-Producing Wells,” *Sensors*, vol.16, no 10, pp:1703-1719, 2016.

[11]W.H. Cui, B. Li, J. Chen and, X.W. Li, “ A Novel Method of Multi-Information Acquisition for Electromagnetic Flow Meters,” Sensors, vol.16, no 25, 2016,doi:10.3390/s16010025.

[12]X. Z. Zhang and Y.T Li, “Calculation of the Virtual Current in an Electromagnetic Flowmeter with One Bubble Using 3D Model,” ISA Transactions, vol. 43,no 2,pp189-194,2004.

[13]O. Cazarez, D. Montoya, A. G. Vital and A. C. Bannwart, “Modeling of Three-phase Heavy Oil-water-gas Bubbly Flow in upward Vertical Pipes,” International Journal of Multiphase Flow, vol.36,no 6,pp439-448,2010.

[14]M.K. Bevir, “The theory of induced voltage electromagnetic flowmeters,” Journal of Fluid Mechanics,vol.43,no 3,pp577-590,2006.

[15]X. Z. Zhang. “Calculation and measurement of the magnetic field in a large diameter electromagnetic Flowmeter,”ISA Transactions,vol.42,no 2,pp167-170, 2003.

[16]A. Michalski, J. Starzynski and S.Wincenciak,“3-D approach to designing the excitation coil of an electromagnetic Flowmeter,” IEEE Transactions on Instrumentation and Measurement,vol.51,no 4,pp 833-839,2002.

[17]C. Rosales, M.L. Sanderson, J. Hemp, “Problems in the theory and design of electromagnetic flowmeters for dielectric liquids. Part 2a: Theory of noise generation by turbulence modulation of the diffuse ionic charge layer near the pipe wall,” Flow Meas. Instrum, vol.13,no 4,pp 155–163, 2002.

[18]C. Rosales, M.L. Sanderson, J. Hemp, “Problems in the theory and design of electromagnetic flowmeters for dielectric liquids. Part 2b: Theory of noise generation by charged particles,”. Flow Meas. Instrum, vol.13,no 4,pp 165–171, 2002.

[19]Q. P. Liu, X. G. Qiao, J. L. Zhao, Z. A. Jia, H. Gao, and M. Shao,“Novel fiber Bragg grating accelerometer based on diaphragm,” IEEE Sensors J., vol. 12, no. 10, pp. 3000-3004, Oct. 2012.

[20]C. Stelian,“Calibration of a Lorentz force flowmeter by using numerical modeling,” Flow Meas. Instrum,vol.33,no 33,pp 36-44,2013.

[21]Stefano Ricci , Valentino Meacci , Beat Birkhofer , Johan Wiklund,“FPGA-Based System for In-Line Measurement of Velocity Profiles of Fluids in Industrial Pipe Flow,” IEEE Transactions on Industrial Electronics,vol.65,no 5,pp 3997-4005, May 2017.

[22]Y. L. Yeow, J. W. Taylor, "Obtaining the shear rate profile of steady laminar tube flow of newtonian and non-Newtonian fluids from nuclear magnetic resonance imaging and laser doppler velocimetry data", J. Rheol., vol. 46, no. 2, pp. 351-365, Mar. 2002.

Liang GE received a B.S. degree and the M.E. degree in Southwest Petroleum University, Chengdu, China in 2007 and 2010, respectively. He is currently pursuing a Ph.D. degree in Measuring and Testing Technology & Instrument at Sichuan University. His current research interests include downhole Instruments and petroleum devices. From 2012 to 2016, he was a Lecturer with the College of Mechanical and Electronic Engineering, SWPU, where he is currently an Associate Professor with the college of Mechanical and Electronic Engineering, SWPU.

Guohui WEI received the B.S. degree in physics from Northwest Normal University and the M.E. degree in radio physics from Xidian University in 1998 and 2006. His current research interests include electromagnetic measuring instruments and antenna design.

Qing Wang received a Ph.D. degree in 2001.Her research interests focus on product life cycle engineering including design and optimization for the product life cycle, computer simulation and advanced manufacturing techniques, electronic instrumentation and measurement. She is currently an Associate Professor at the School of Engineering and Computing Sciences, Durham University, U.K.

Ze HU received a Ph.D. degree in 1996; he has published more than 30 research articles. His current research interests include electronic information and down-hole testing. He is currently a Professor at the school of Electronic and Information Engineering, Southwest Petroleum University.

Junlan LI received a B.S. degree in Communication Engineering from Yangtze University and the M.E. degree in Measuring and Testing Technology & Instrument from Southwest Petroleum University in 2007 and 2010. Her current research interests include sensor design and signal detection.